



Letters

A residual heat compensation based scan strategy for powder bed fusion additive manufacturing

H. Yeung*, B. Lane

National Institute of Standards and Technology, Gaithersburg, MD 20899, United States



ARTICLE INFO

Article history:

Received 25 February 2020

Received in revised form 4 June 2020

Accepted 17 July 2020

Available online 31 July 2020

Keywords:

Feedforward control

In-situ melt-pool monitoring

Continuous laser power variation

ABSTRACT

Typical scan strategies for laser powder bed fusion (LPBF) additive manufacturing systems apply a constant laser power and scan speed. Localized preheating from adjacent scan paths (residual heat) result in inconsistent melt-pool morphology. A new control approach is proposed which compensates the residual heat through laser power adjustment. A model called residual heat factor (RHF) is developed to 'quantify' the residual heat effect, and laser power is controlled proportional to this RHF. Experiments are conducted on a custom-controlled LPBF testbed on nickel-alloy (IN625) bare plate, and the effects of this unique scan strategy are investigated by in-situ melt-pool monitoring.

Published by Elsevier Ltd on behalf of Society of Manufacturing Engineers (SME).

1. Introduction

Laser powder bed fusion (LPBF) additive manufacturing (AM) uses a high-power laser to melt and solidify thin layers of metal powder in geometric patterns sliced from parts' solid models. A typical LPBF process scans the laser back and forth with constant power and speed in a 'hatch' pattern to cover each layer. Reheating from adjacent scan paths, or heat accumulation result in inconsistent melt-pool morphology due to dynamic thermal history [1]. This dynamic thermal process can elicit heterogeneities in the solidified microstructure [2,3], or defects such as end-of-track key-hole pores [4,5].

Limited research demonstrates practical methods to alleviate these heterogeneities through laser power or scan strategy control, which requires custom research testbeds [5–8]. Earlier, the authors formulated a geometric conduction factor (GCF), which approximates the effect of geometry-based heat accumulation due to small solidified volumes enclosed by powder [8]. Laser power was controlled proportionally to GCF which improved surface finish. This paper introduces a new factor, called the residual heat factor (RHF), which accounts for the dynamic reheating effect. We present an RHF-based model for power control strategy, and experimental optimization of RHF parameters reduce melt-pool size variability.

2. AM process control and monitoring

AM process preparation can be divided into four major steps: (1) Digitally slice parts' solid models into layers. (2) Assign scan path/vectors for each layer. (3) Interpolate scan vectors into time-stepped digital position commands, which may also include other auxiliary information (explained below). (4) Send the digital commands to AM machine controller to execute. Fig. 1a shows the digital command format used on the National Institute of Standards and Technology (NIST) Additive Manufacturing Metrology Testbed (AMMT) [9,10]. The digital command is a $n \times m$ numerical array, where n is the number of time steps in 10 μ s increments, and m is the number of control parameters. This format is based on the xy2-100 protocol for laser-galvo position (X, Y), but extends it to control laser power (L), laser spot size (D), and triggers (T) for synchronizing process monitoring sensors, such as a coaxial melt-pool monitoring (MPM) camera shown in Fig. 1a [11]. The digital command file enables full description of the scan strategy and the geometry of a part [8]. On most commercial systems, neither access nor control of this digital command file is typically available.

The MPM camera used in AMMT captures melt-pool incandescent emission diverted by a dichroic mirror and filtered at the emission bandwidth of (850 ± 20) nm. The custom optics enable 1:1 magnification and 8 μ m/pixel. Since MPM images and galvo positions are synchronized, the calculated melt-pool area can be plotted against their XY position as shown in Fig. 1b. The temporal variation of melt-pool image area (in pixels) is used here as a metric for melt-pool uniformity. The AMMT uses the digital command

* Corresponding author.

E-mail address: ho.yeung@nist.gov (H. Yeung).

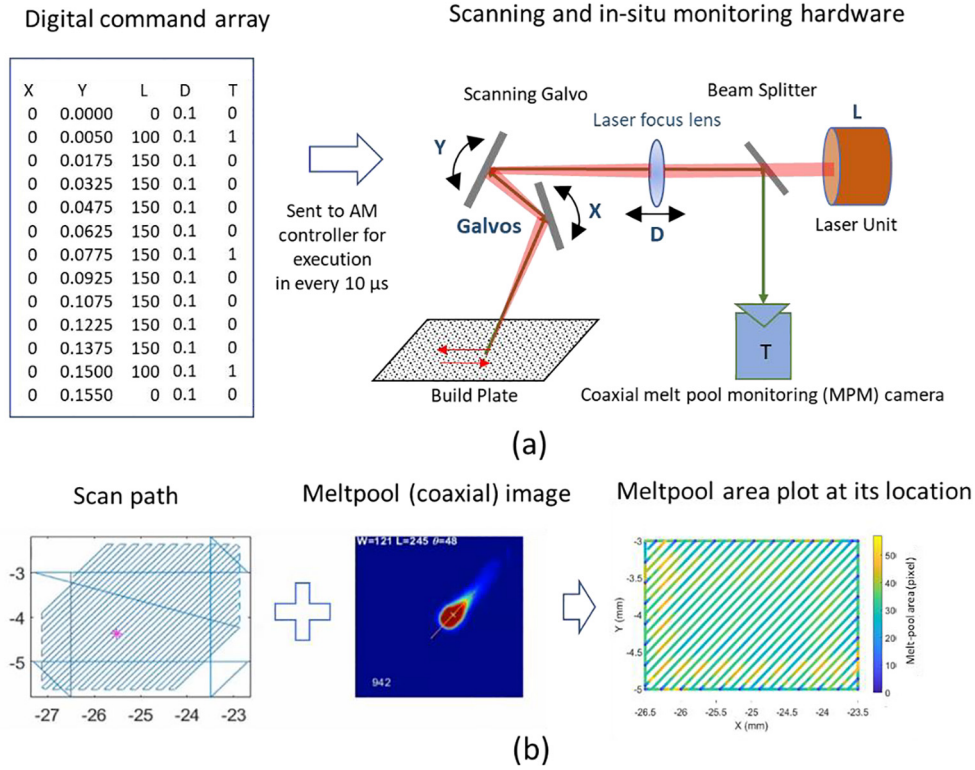


Fig. 1. In-situ MPM image registration. (a) Images fully synchronized with laser positions through digital commands. (b) MPM pixel values and area superimposed over the location they were taken.

file as an intermediate interface file, making it accessible, editable, or available for spatial registration of process monitoring data, as in Fig. 1b.

3. Example residual heat effect under constant laser power

Melt-pool morphology is an important process signature indicating the level of process stability. To demonstrate the effect of dynamic residual heat on melt-pool morphology, a 3 mm × 2 mm rectangular area (Fig. 2) was scanned on a nickel alloy (IN625) bare metal plate with constant laser power of 195 W, scan speed of 1000 mm/s, laser spot size of 85 μm in diameter, and hatch spacing of 0.1 mm. To maintain constant speed during the build, the scan lines are programmed to overshoot (skywrite) when changing directions (blue lines in Fig. 2a). Over-

shoot time is 4.24 ms here. The MPM camera captured 20,000 frames/s, and melt-pool area within each frame is plotted in Fig. 2b. This shows a clearly heterogeneous melt-pool size despite constant process parameters, primarily due to the residual heat effect.

4. Residual heat factor (RHF)

The scan path is made of discrete points defined by the digital command (Fig. 3a). The preheating on point i by a previously scanned point k is assumed dependent on three factors: (1) distance between i and k (d_{ik}), (2) elapsed time since k was scanned (t_{ik}), and (3) the laser power (L_k) at point k . Specified time T and radius R threshold values ignore points scanned too long ago or too far away. A numerical value, referred to as residual heat factor

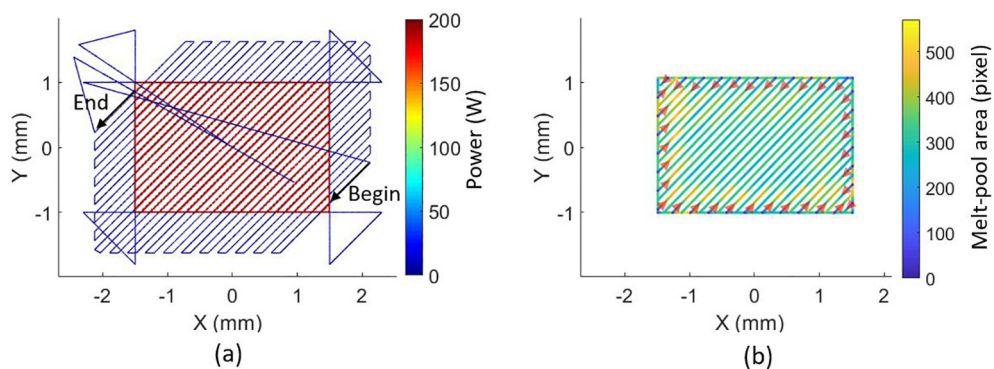


Fig. 2. Melt-pool variation under constant laser power and speed. (a) Programmed laser power. (b) Resulting melt-pool area mapped to XY position. Red arrows indicate where each scan line starts, which coincides with the locations of the larger melt-pool size. (For interpretation of the references to colour in this figure legend, the reader is referred to the web version of this article.)

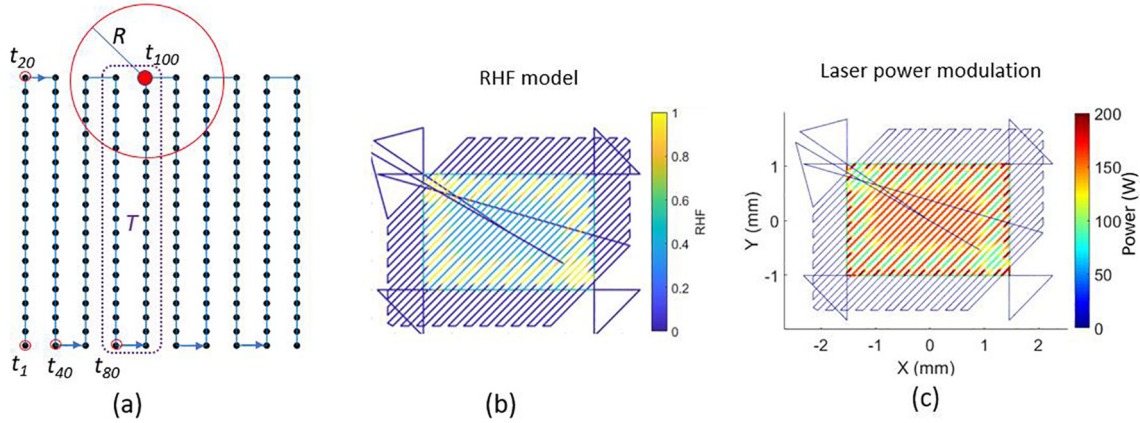


Fig. 3. Residual heat factor. (a) Discretized scan path from digital command. Elapsed time $< T$ is indicated by purple dotted line and distance $< R$ indicated by red circle. (b) RHF model developed from the scan strategy in Fig. 2 with $R = 0.29$ mm and $T = 6$ ms. (c) Laser power adjusted based on RHF model in (b). (For interpretation of the references to colour in this figure legend, the reader is referred to the web version of this article.)

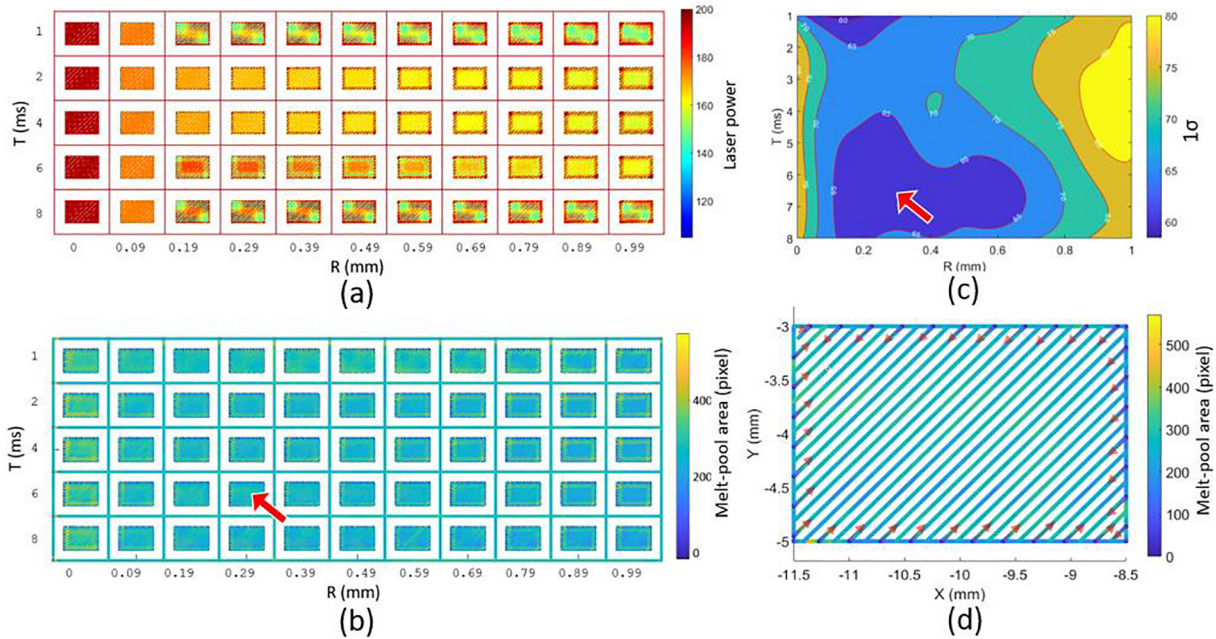


Fig. 4. RHF parameter optimization. (a) RHF adjusted laser power plots in (R,T) parameter space. (b) Corresponding measured melt-pool areas. (c) Spline interpolation of the melt-pool area variability (1σ) . (d) Enlarged view of the melt-pool area plot for the location indicated by the arrows in (b) and (c).

(RHF) defined by Eq. (1), may be assigned to each point to describe this reheating condition, where S_i is the set of previous scanned points, $S_i = \{t_{ik} < T \cap d_{ik} < R, \text{ where } i > k\}$ as shown in Fig. 3a. S_i is empty while $R = 0$ mm.

$$RHF_i = \sum_{k \in S_i} \left(\frac{R - d_{ik}}{R} \right)^2 \left(\frac{T - t_{ik}}{T} \right) L_k \quad (1)$$

Eq. (1) assumes the reheating is linearly proportional to time and square-proportional to distance. R and T values are chosen as tuning parameters, and RHF value is computed for each point listed in the digital command file. Fig. 3b demonstrates normalized RHF for the scan described by Fig. 2a with $R = 0.29$ mm and $T = 6$ ms, which generally replicates the melt-pool area variation in Fig. 2b. The commanded laser power L is adjusted based on the RHF according to Eqs. (2) and (3), where L_0 = original laser power, C = power adjustment factor, and RHF_N = normalized RHF. The three tuning parameters R , T and C are optimized by observing

their relative effect on the experimental temporal variation of the melt-pool size as explained below. C is heuristically set to 0.25, resulting in a laser power range of 146.25 W to 195 W. Fig. 3c plots the adjusted laser power.

$$L = L_0 \cdot ((1 - C) + C \cdot (1 - RHF_N)) \quad (2)$$

$$RHF_N = \min \left(\frac{RHF}{\text{mean}(RHF) + \text{std}(RHF)}, 1 \right) \quad (3)$$

5. Experimentally tuning RHF

For experimental optimization, the laser power is adjusted based Eqs. (1)–(3) using a range of $R = 0$ mm to 0.99 mm and $T = 1$ ms to 8 ms, as shown in Fig. 4a. $R = 0$ mm (hence all S_i is empty) is equivalent to baseline (constant power). A total of 55

rectangles scanned, with 5 as baseline and 50 with RHF-based laser power control.

Fig. 4b shows the measured melt-pool area maps corresponding to these conditions. The standard deviation of melt-pool area (in pixels) is calculated for each (R,T) combination, and cubic-spline interpolated to form the contour plot in Fig. 4c. Minimum melt-pool area variation with $\sigma = 60.5$ pixels was determined at $R = 0.29$ mm and $T = 6$ ms (indicated with arrow), resulting in 27% reduction compared with the baseline ($\sigma = 76.7$ pixels). RHF-optimized melt-pool area plot in Fig. 4d shows visible improvement compared to the baseline plot Fig. 2b.

Fig. 4c shows that effective values of (R,T) are bounded by [0.1 mm to 0.7 mm, 4.5 ms to 8 ms]. Under similar laser parameters and material, melt pool length and width was 0.75 mm and 0.1 mm, respectively [12]. Overshoot (skywriting) time between tracks when the laser turns off and the melt pool cools was 4.24 ms. Though not conclusive, these indicate R and T are on the same dimensional scale as melt pool phenomena.

6. Summary and future work

Better laser power control in LPBF has potential to reduce defects, control residual stress or microstructure, or improve the processing speed. A residual heat factor (RHF) model was developed, which simplifies the dynamic reheating effect of a scanned melt-pool into a single parameter. Laser power was continuously adjusted based on RHF to reduce local variability of melt-pool area measured via coaxial camera by 27% compared to baseline. While melt-pool area was used as an objective to optimize RHF parameters here, future efforts will combine geometry [8] and reheating based control parameters to optimize other part qualities.

Declaration of Competing Interest

The authors declare that they have no known competing financial interests or personal relationships that could have appeared to influence the work reported in this paper.

References

- [1] Heigel J, Lane B, Phan T, Brown D, Strantzla M, Levine L. Sample design and in-situ characterization of cooling rate and melt pool length during 3D AM builds of 15-5 and IN625 AM-Bench artifacts. *Integrating Mater Manuf Innov* 2019.
- [2] Criales LE, Arisoy YM, Lane B, Moylan S, Donmez A, Özel T. Laser powder bed fusion of nickel alloy 625: experimental investigations of effects of process parameters on melt pool size and shape with spatter analysis. *Int J Mach Tools Manuf* 2017;121:22–36. <https://doi.org/10.1016/j.ijmactools.2017.03.004>.
- [3] Stoudt MR, Williams ME, Levine LE, Creuziger A, Young SA, Heigel JC, Lane BM, Phan TQ. Location-specific microstructure characterization within IN625 additive manufacturing benchmark test artifacts. *Integr Mater Manuf Innov* 2020;9(1):54–69. <https://doi.org/10.1007/s40192-020-00172-6>.
- [4] Martin AA, Calta NP, Khairallah SA, Wang J, Depond PJ, Fong AY, et al. Dynamics of pore formation during laser powder bed fusion additive manufacturing. *Nat Commun* 2019;10:1–10. <https://doi.org/10.1038/s41467-019-10009-2>.
- [5] Wang Q (Pan) Michaleris P, Nassar AR, Irwin JE, Ren Y, Stutzman CB. Model-based feedforward control of laser powder bed fusion additive manufacturing. *Addit Manuf* 2020;31:100985. <https://doi.org/10.1016/j.addma.2019.100985>.
- [6] DePond PJ, Guss G, Ly S, Calta NP, Deane D, Khairallah S, et al. In situ measurements of layer roughness during laser powder bed fusion additive manufacturing using low coherence scanning interferometry. *Mater Des* 2018;154:347–59. <https://doi.org/10.1016/j.matdes.2018.05.050>.
- [7] Phillips T, Fish S, Beaman J. Evaluation of a feed-forward laser control approach for improving consistency in selective laser sintering. In: *Proc. Solid Free. Fabr. Symp., Austin, Texas.* p. 1673–81.
- [8] Yeung H, Lane B, Fox J. Part geometry and conduction-based laser power control for powder bed fusion additive manufacturing. *Addit Manuf* 2019;30. <https://doi.org/10.1016/j.addma.2019.100844>.
- [9] Lane et al. Design, Developments, and Results from the NIST Additive Manufacturing Metrology Testbed (AMMT). *Solid Free Fabr 2016 Proc 26th Annu Int Solid Free Fabr Symp* (n.d.).
- [10] Yeung H, Lane BM, Donmez MA, Fox JC, Neira J. Implementation of advanced laser control strategies for powder bed fusion systems. *Procedia Manuf* 2018;26:871–9. <https://doi.org/10.1016/j.promfg.2018.07.112>.
- [11] Lane B, Yeung H. Process monitoring dataset from the additive manufacturing metrology testbed (AMMT): “3d scan strategies”. *J Res Natl Inst Stand Technol* 2019;124.
- [12] Lane B, Heigel J, Ricker R, Zhirnov I, Khromschenko V, Weaver J, et al. Measurements of melt pool geometry and cooling rates of individual laser traces on IN625 bare plates. *Integrating Mater Manuf Innov* 2020. <https://doi.org/10.1007/s40192-020-00169-1>.